

# ADVANCED FUNCTIONAL MATERIALS

## Supporting Information

for *Adv. Funct. Mater.*, DOI: 10.1002/adfm.201404311

Novel Polygonal Vanadium Oxide Nanoscrolls as Stable  
Cathode for Lithium Storage

*Qiulong Wei, Shuangshuang Tan, Xiaoyi Liu, Mengyu  
Yan, Fengchao Wang, Qidong Li, Qinyou An, Ruimin Sun,  
Kangning Zhao, Hengan Wu, and Liqiang Mai\**

Copyright WILEY-VCH Verlag GmbH & Co. KGaA, 69469 Weinheim, Germany, 2013.

## Supporting Information

### **Novel Polygonal Vanadium Oxide Nanoscrolls as Stable Cathode for Lithium Storage**

*Qiulong Wei, Shuangshuang Tan, Xiaoyi Liu, Mengyu Yan, Fengchao Wang, Qidong Li, Qinyou An, Ruimin Sun, Kangning Zhao, Hengan Wu, and Liqiang Mai\**

Mr. Q.L. Wei,<sup>[†]</sup> S.S. Tan,<sup>[†]</sup> M.Y. Yan, Q.D. Li, Ms. R.M. Sun, Mr. K.N. Zhao, Prof. L.Q. Mai

State Key Laboratory of Advanced Technology for Materials Synthesis and Processing

WUT-Harvard Joint Nano Key Laboratory

Wuhan University of Technology, Hubei, Wuhan 430070, China

Mr. X.Y. Liu, Dr. F.C. Wang, Prof. H.A. Wu

CAS Key Laboratory of Mechanical Behavior and Design of Materials

Department of Modern Mechanics

University of Science and Technology of China, Hefei, Anhui 230027, China

Dr. Q.Y. An

Cullen College of Engineering, Department of Electrical & Computer Engineering

University of Houston, Houston, USA

[†] Q.L. Wei and S.S. Tan contributed equally to this work

**The SI file includes detailed Experimental Methods, 3 Tables and 17 Figures.**

**Materials.**  $V_2O_5$  powder and organic alkanols were analytical pure and purchased from Sinopharm Chemical Reagent Co., Ltd. (Shanghai, China) and used as received.

**Experimental Methods.** The  $V_2O_5$  sols were prepared by a melt quenching process as reported previously.<sup>[1]</sup> The vanadium oxide polygonal nanoscrolls (PNSs) were synthesized via a facile hydrothermal method. The  $V_2O_5$  sols (0.2 mmol) were diluted with deionized water at room temperature under magnetic stirring for 2 h. Then 1,2-propanediol (5  $\mu$ l) was added in the diluted solution under magnetic stirring for another 2 h. Then mixed solution was transferred into a sealed Teflon container with and statically heated in oven at 180 °C for 36 h and then allowed to cool to room temperature naturally. The green precipitation product was washed with deionized water and alcohol **each three times**, and then dried at 70 °C for 24 h. The preparation of the ultrathin nanobelts was with a reactant concentration of  $V_2O_5$  sols (0.5 mmol) and kept other same condition with the synthesis of PNSs. The nanowires were synthesized with a reactant concentration of  $V_2O_5$  sols (1.0 mmol). Another control experiment was undertaken but with different small organic alkanol molecules.

**Materials Characterization.** X-ray diffraction (XRD) data of sample were collected with a D8 Advance X-ray diffractometer with area detector, using Cu  $K\alpha$  radiation ( $\lambda = 1.5418 \text{ \AA}$ ) in a  $2\theta$  range from 5° to 70°. The microstructures were observed by Field-emission scanning electron microscopy (FESEM) (JEOL-7100F), and transmission electron microscopy (TEM) and high-resolution transmission electron microscopy (HRTEM) (JEM-2100F). Raman spectra were obtained using a Renishaw INVIA micro-Raman spectroscopy system and FT-IR spectra were obtained using a Nexus system. X-ray photoelectron spectroscopy (XPS) measurements were obtained using a VG MultiLab 2000 instrument. Thermogravimetric analysis (TGA) was performed using a Netzsch STA 449C simultaneous analyzer. **Brunauer-Emmet-Teller (BET) surface areas were measured by using Tristar II 3020 instrument.**

**Electrochemical measurements.** The electrochemical properties were characterized by assembly of **2016-type coin cells** with lithium metal foil as the anode in a glovebox filled with

pure argon gas. The cathode electrodes were composed of 70% active material, 20% acetylene black and 10% poly (tetrafluoroethylene) (PTFE) binder. The mixture was dispersed in isopropanol for better blending. And the mixed clay was rolled to produce flexible, freestanding film. Then the film was punched into circular disk and dried at 70 °C for 24 h. The electrode loading was 2–3 mg/cm<sup>2</sup>. A solution (1 M) of LiPF<sub>6</sub> in EC/DMC (1:1 vol/vol) was used as the electrolyte. The cells were aged for 12 h before charge/discharge to ensure full absorption of the electrolyte into the electrodes. Galvanostatic charge/discharge measurement was performed by a multichannel battery testing system (LAND CT2001A), electrochemical impedance spectroscopy (EIS) were tested with an Autolab Potentiostat Galvanostat (PGSTAT302N). All the measurements were carried out at room temperature.

#### **Details of finite element model simulation.**

We set a series of 2D finite element models to simulate the elastic mechanical behavior of the polygonal nanoscrolls by using COMSOL Multiphysics.<sup>[2]</sup> The Young modulus and poisson ratio of nanoscroll is set as 100 GPa and 0.2, respectively. Free quad mesh is defined in all models. The stress–strain relationship is given by equation:  $\sigma - \sigma_0 = D\varepsilon$ , where  $D$  is the elasticity matrix and  $\sigma_0$  is the initial stress. The direct stationary nonlinear solver (MUMPS) is used to solve the balance equations. In our simulations, an isotropic initial stress of 1000 Pa is applied in the domain of nanoscroll to simulate the diffusion-induced stress resulting from the ion intercalation. The thickness of nanoscroll is 15 nm. We considered two kinds of boundary conditions. The first one is that the inner boundary of the polygonal nanoscroll was held fixed while the outer boundary was set to be free. The second one is just the opposite, which means the outer boundary was fixed while the inner boundary was free. As is well-known, stress concentration is one of the crucial factors that cause fatigue undermine of the polygonal nanoscrolls. The stress concentration can be observed distinctly near the inside corners for all the models, as shown in Figure S17. Moreover, our simulations also calculated the maximum von Mises stress for various structures under different boundary conditions, which are listed

in Table S3. These results indicate that the fatigue undermine is more likely to happen in the trapezoidal nanoscrolls. We believe that the simulation will be helpful for the design of suitable shape and structure in the future.

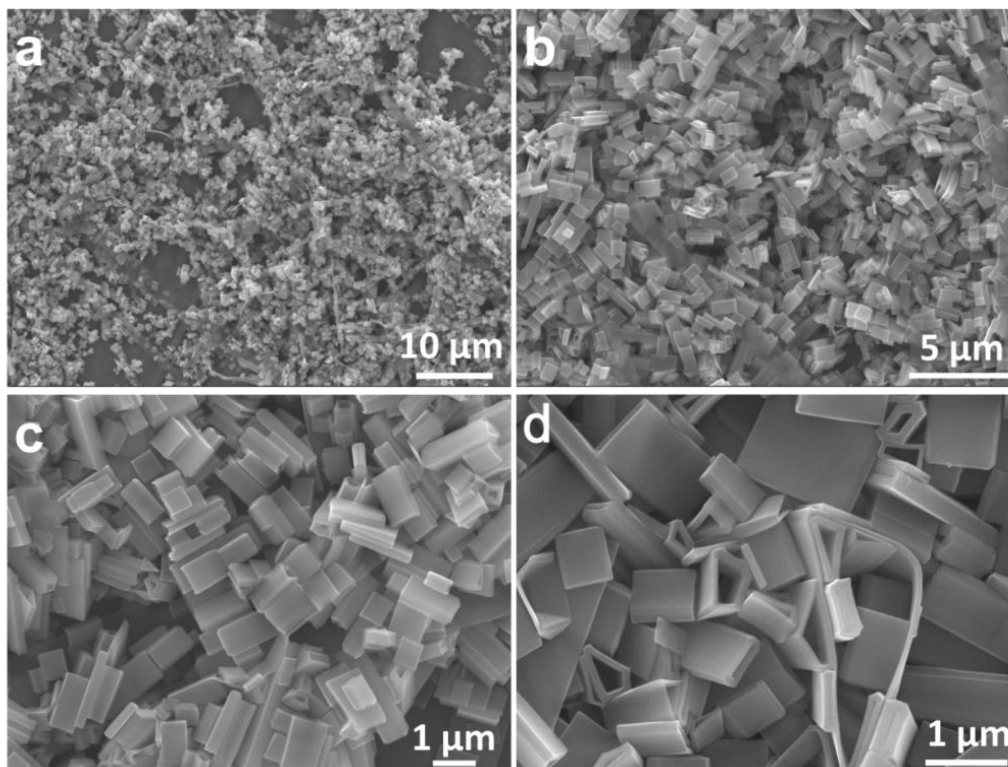


**Figure S1.** (a-d) FESEM images of the PNSs.

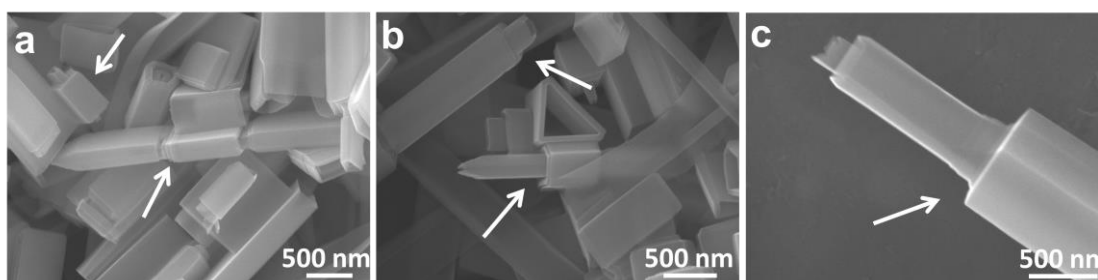


**Figure S2.** (a-c) FESEM images of the scroll-by-scroll coaxial scrolls.

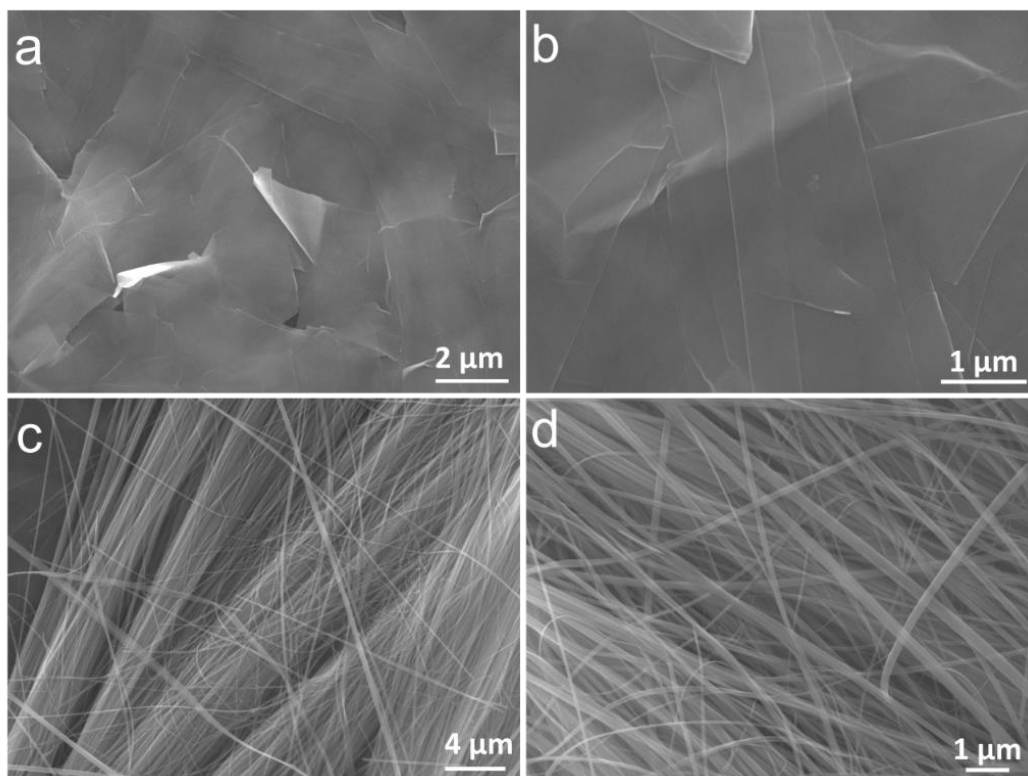


**Figure S3.** FESEM images of the UNBs (a,b) and NWs (c,d), respectively.

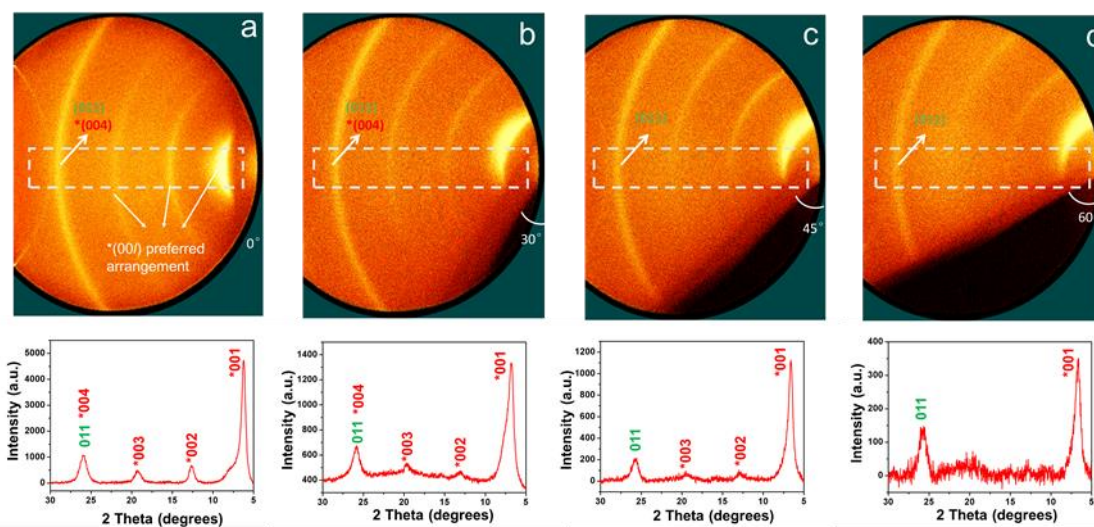


**Figure S4.** The XRD 2D images and related patterns of PNSs obtained at various psi-axis angle,  $0^\circ$  (a),  $30^\circ$  (b),  $45^\circ$  (c), and  $60^\circ$  (d).

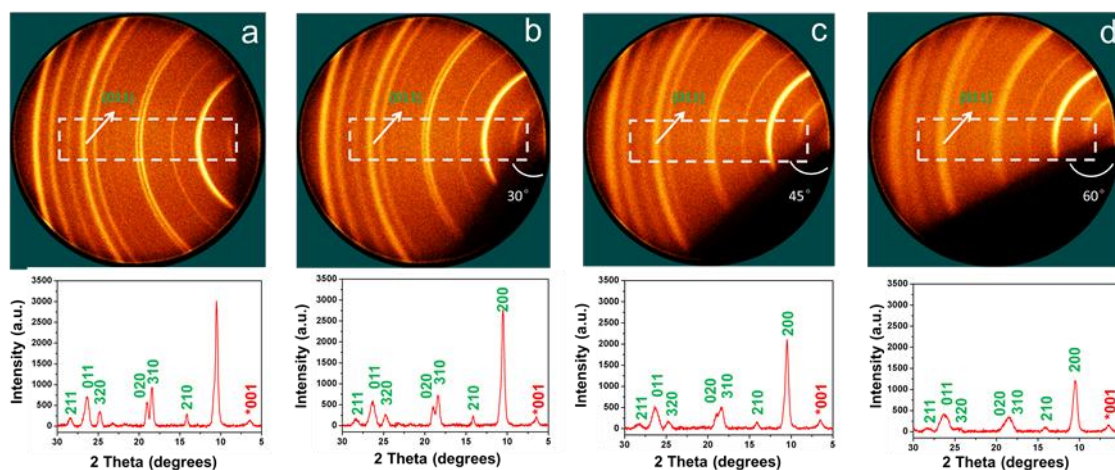


**Figure S5.** The XRD 2D images and related patterns of NWs obtained at various psi-axis angle,  $0^\circ$  (a),  $30^\circ$  (b),  $45^\circ$  (c), and  $60^\circ$  (d).

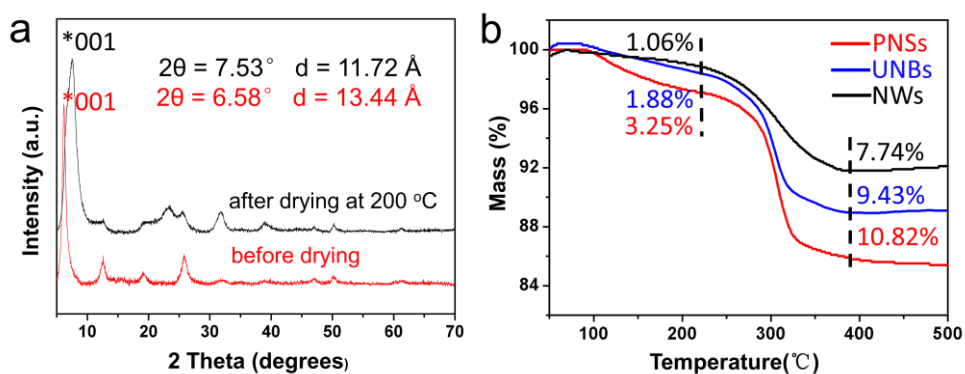


**Figure S6.** (a) XRD patterns of the PNSs and before and after drying at  $200^\circ\text{C}$  for 8 h. (b) The TGA analysis of the three samples, measured in  $\text{N}_2$  atmosphere.

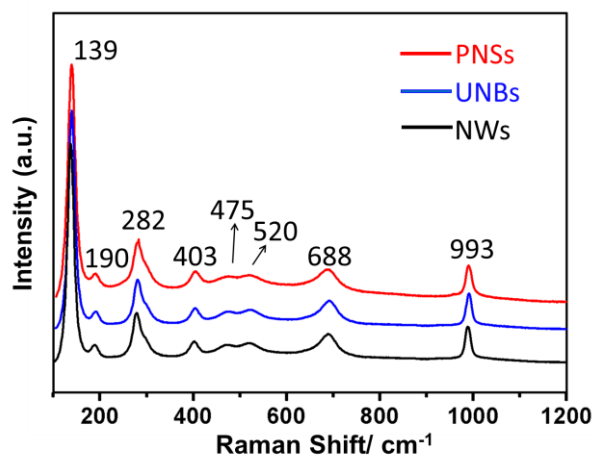


**Figure S7.** Raman spectra of the PNSs, UNBs and NWs. The Raman spectra of the samples are conformed to the previous literature.<sup>[3-5]</sup> The peaks located at 139 and 190  $\text{cm}^{-1}$  are assigned to the stretching mode of  $(\text{V}_2\text{O}_2)_n$  which correspond to the chain translation.<sup>[6]</sup> The peak is strongly associated with the layer structure.<sup>[6]</sup> The peaks located at 282 and 403  $\text{cm}^{-1}$  are assigned to the bending vibration of the V=O bonds.<sup>[7]</sup> The peak at 520  $\text{cm}^{-1}$  is assigned to the triplycoordinated oxygen ( $\text{V}_3\text{-O}$ ) stretching mode which results from edge shared oxygen in common to three pyramids. The peaks at 688  $\text{cm}^{-1}$  are assigned to the doubly coordinated oxygen ( $\text{V}_2\text{-O}$ ) stretching and bending vibration mode which results from corner-shared oxygen in common to two pyramids, respectively.<sup>[8]</sup> While the peak at 993  $\text{cm}^{-1}$  corresponds to the terminal oxygen (V=O) stretching mode which results from an unshared oxygen.<sup>[9]</sup> The results demonstrates that the three samples have the same  $\text{V}_3\text{O}_8$  layer stack behaviors.

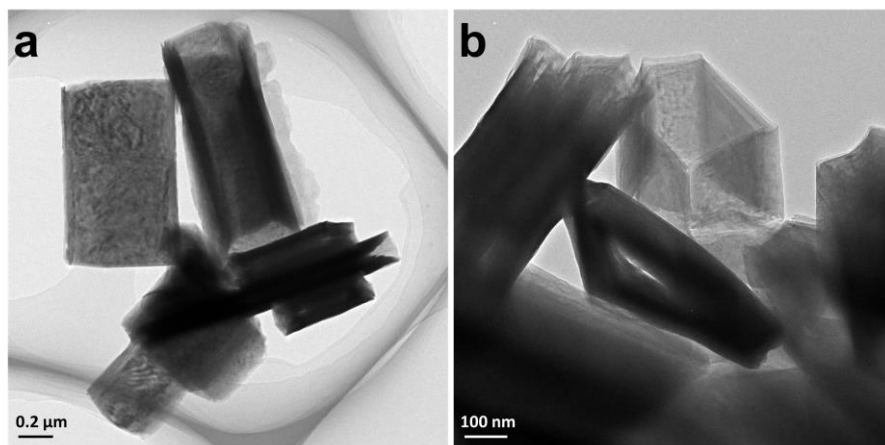


**Figure S8.** (a,b) TEM images of the PNSs.

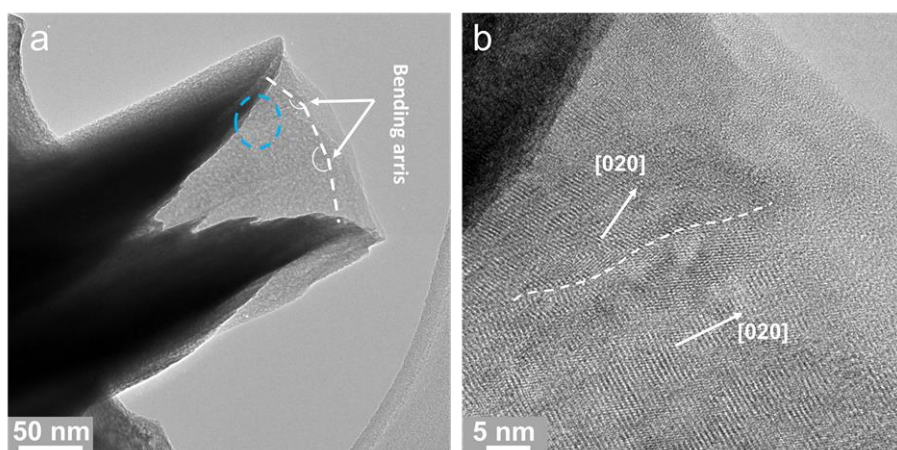


**Figure S9.** (a) TEM image of a caritive end of the PNS, which shows clear bending folds. (b) HRTEM image displays a folded line and lattice fringe shifts.

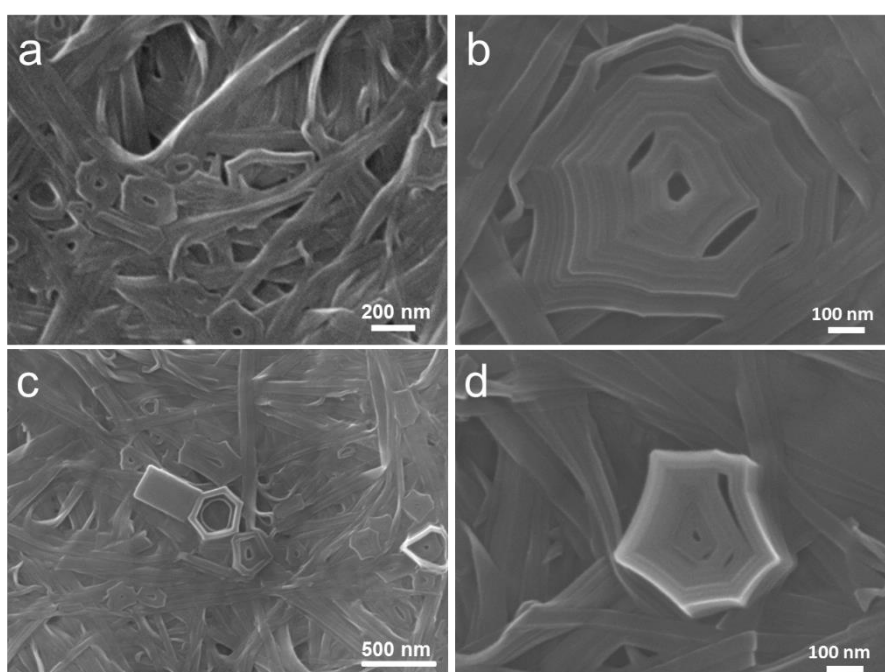


**Figure S10.** FESEM images of the PNSs after hydrothermal for 12 hours (a, b) and 16 hours (c, d).

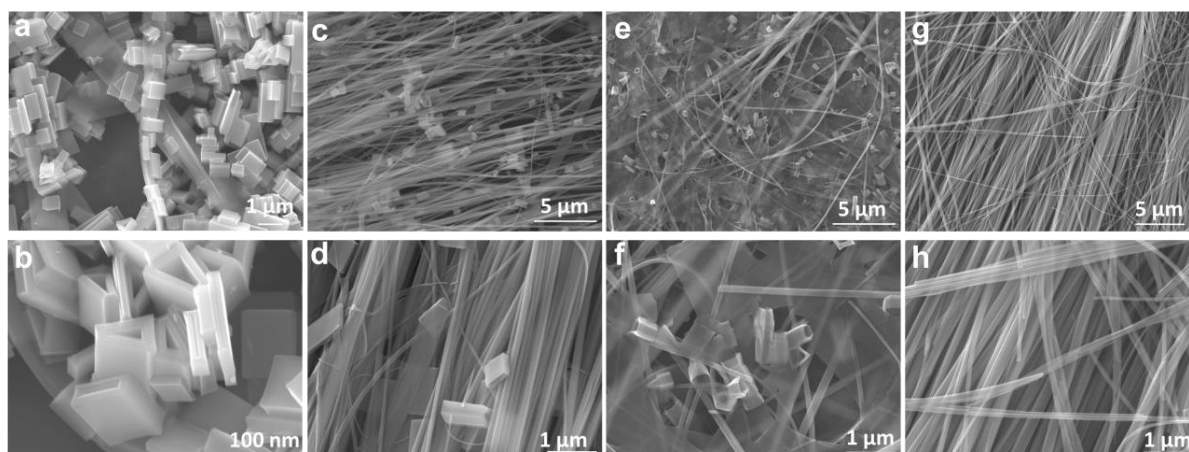


**Figure S11.** FESEM images of the samples under different amount of 1,2-PDO: 6 $\mu$ l (a, b), 7 $\mu$ l (c, d), 8 $\mu$ l (e, f), 15 $\mu$ l (g, h).

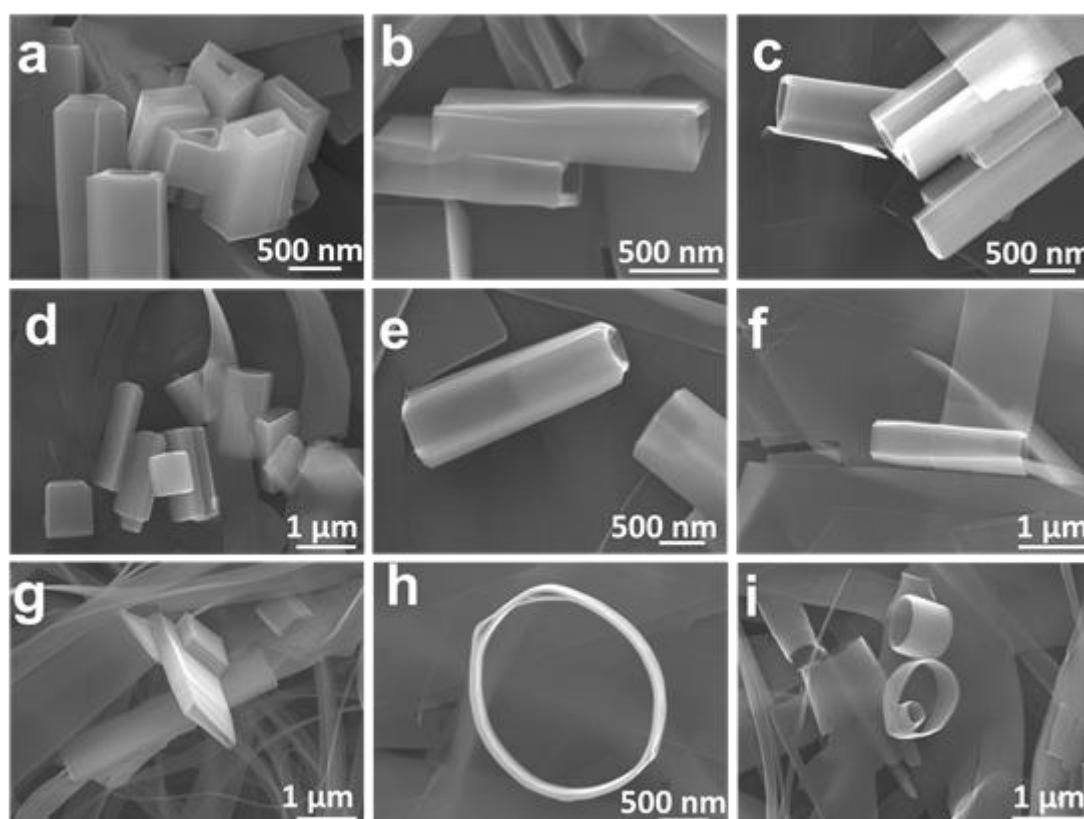


**Figure S12.** FESEM images of the samples under the same experimental conditions but use the alcohols with the different alkyl-chain lengths and different hydroxyl amount: n-propyl alcohol (a), isopropanol (b), 1,3-propanediol (c), glycerol (d), n-butyl alcohol (e), n-amyl alcohol (f), n-hexanol (g), 1-octanol (h), and 1-cetanol (i).

**Table S1.** The shape of the scroll and the molar ratio (alcohol:V) of the reaction, which used the alcohols with the different alkyl-chain lengths and different hydroxyl amount. The molar amount of  $V_2O_5$  sols is 0.2 mmol in all of the above reaction.

surfactant	$C_nH_{2n+2}O_x$	alcohol:V	the shape of the scroll
ethanol	$n=2, x=1$	1:4.7	no scroll
glycol	$n=2, x=2$	1:4.5	no scroll
n-propyl alcohol	$n=3, x=1$	1:6.0	polygonal
isopropanol	$n=3, x=1$	1:6.2	polygonal
1,2-propanediol	$n=3, x=2$	1:5.8	polygonal
1,3-propanediol	$n=3, x=2$	1:4.8	polygonal
glycerol	$n=3, x=3$	1:4.8	polygonal
n-butyl alcohol	$n=4, x=1$	1:6.1	polygonal
1, 4-butanediol	$n=4, x=2$	1:4.9	polygonal
n-amyl alcohol	$n=5, x=1$	1:7.2	polygonal
n-hexanol	$n=6, x=1$	1:8.4	polygonal
1-octanol	$n=8, x=1$	1:4.2	circular
1-cetanol	$n=16, x=1$	1:5.8	circular

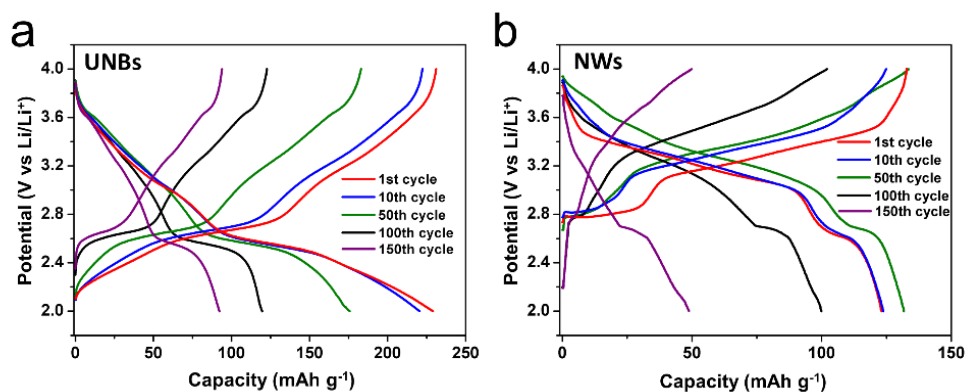


**Figure S13.** Charge–discharge curves of the UNBs (a) and the NWs (b) cathodes cycled at  $0.1 \text{ A g}^{-1}$  in 2–4 V at different cycles.

**Table S2.** The BET surface area of the PNSs, UNBs and NWs.

sample	PNSs	UNBs	NWs
BET surface area ( $\text{m}^2 \text{ g}^{-1}$ )	13.09	15.78	20.63

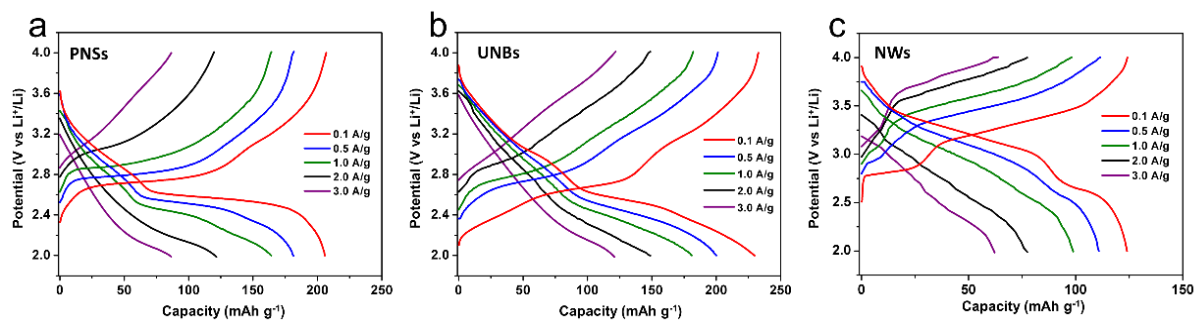


**Figure S14.** Charge–discharge curves of the PNSs (a), UNBs (b) and NWs (c) cathodes cycled at a various charge–discharge rates ranging from 0.1 to 3.0 A g<sup>-1</sup>.

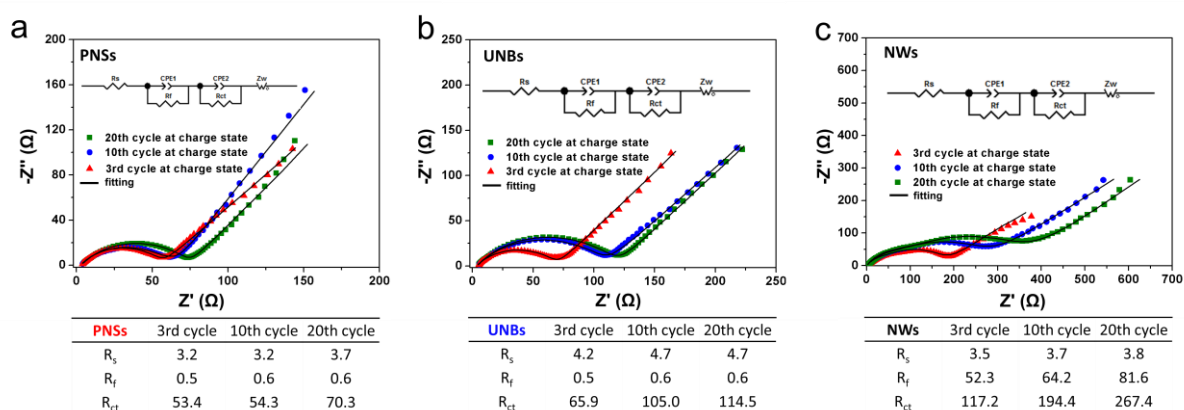


**Figure S15.** The electrochemical impedance spectra (EIS) of the PNSs (a), UNBs (b), and NWs (c) cathodes at various cycles.

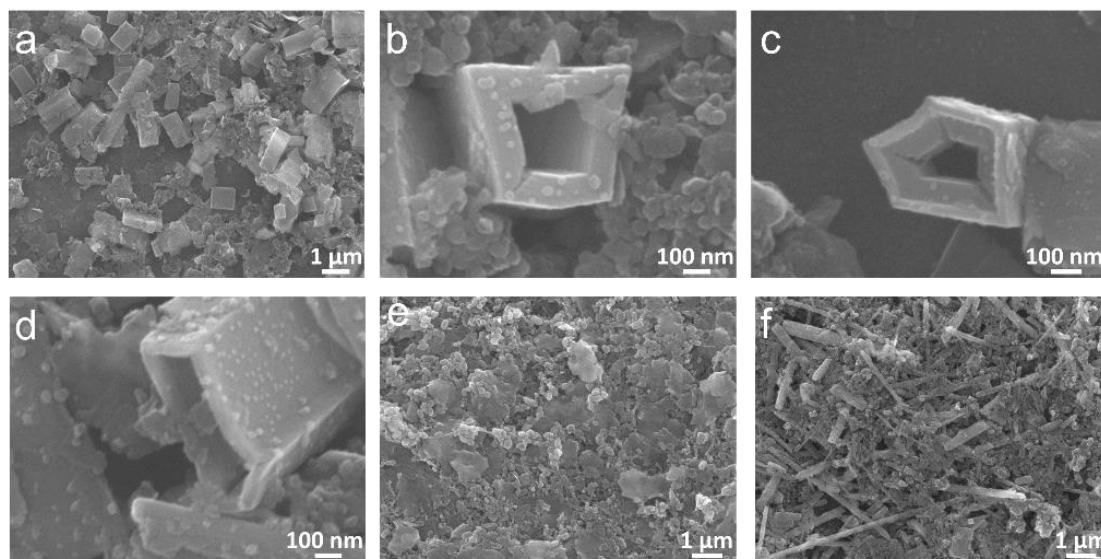


**Figure S16.** FESEM images of the PNSs (a-d), UNBs (e) and NWs (f) cathodes after 150 cycles.

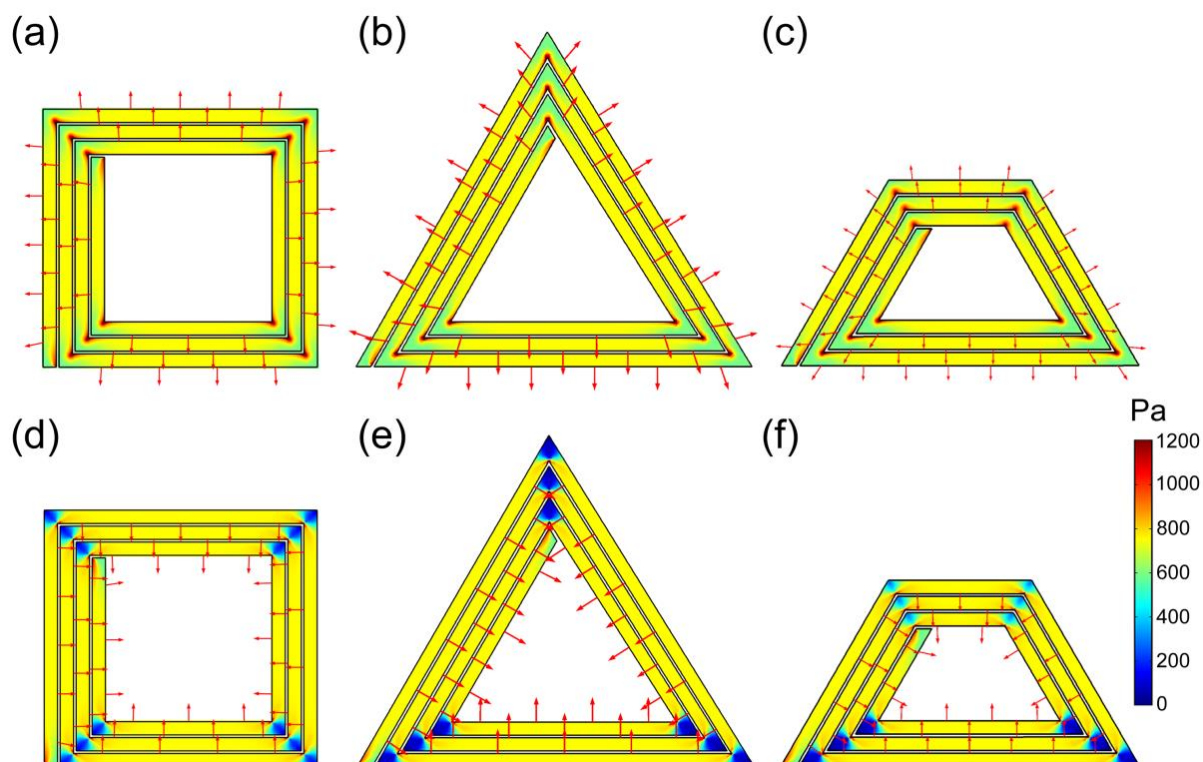


**Figure S17.** The calculated von Mises stress contour for rectangular (a,d), triangular (b,e) and trapezoidal (c,f) nanoscrolls under different boundary conditions. The stress concentration can be observed distinctly near the inside corners for all the models. The arrows illustrate the displacement direction of the free boundaries. If the inner boundary of the polygonal nanoscroll was held fixed (a-c), the outer boundary expands outwards. While for the fixed outer boundary conditions (d-f), the inner boundary expands inwards.

**Table S3.** Maximum von Mises stress for various models.

	Fixed inner boundary (Pa)	Fixed outer boundary (Pa)
rectangular nanoscroll	2571.6	2571.6
triangular nanoscroll	2885.6	2253.0
trapezoidal nanoscroll	3167.9	3186.7

## References

- [1] C. Zhou, L. Mai, Y. Liu, Y. Qi, Y. Dai, W. Chen, *J. Phys. Chem. C*, **2007**, 111, 8202.  
 [2] COMSOL Multiphysics Version 4.2, User's Guide and Reference Guide. Stockholm, **2005**

- [3] K. Zhu, X. Yan, Y. Zhang, Y. Wang, A. Su, X. Bie, D. Zhang, F. Du, C. Wang, G. Chen, *ChemPlusChem* **2014**, 79, 447.
- [4] I. Mjejri, N. Etteyeb, F. Sediri, *Mater. Res. Bull.* **2013**, 48, 3335.
- [5] I. Mjejri, N. Etteyeb, F. Sediri, *J. Alloy. Compound.* **2014**, 611, 372.
- [6] C. Julien, G. Nazri, O. Bergström, *Phys. Status Solidi B* **1997**, 201, 319.
- [7] X. Liu, C. Huang, J. Qiu, Y. Wang, *Appl. Surf. Sci.* **2006**, 253, 2747.
- [8] W. Chen, L. Mai, J. Peng, Q. Xu, Q. Zhu, *J. Solid State Chem.* **2004**, 177, 377.
- [9] S. De, A. Dey, S. De, *J. Phys. Chem. Solids* **2007**, 68, 66.